



NRC Publications Archive Archives des publications du CNRC

Connection between phase diagram, structure and ion transport in liquid, aqueous electrolyte solutions of lithium chloride

Yim, Chae-Ho; Abu-Lebdeh, Yaser A.

This publication could be one of several versions: author's original, accepted manuscript or the publisher's version. / La version de cette publication peut être l'une des suivantes : la version prépublication de l'auteur, la version acceptée du manuscrit ou la version de l'éditeur.

For the publisher's version, please access the DOI link below. / Pour consulter la version de l'éditeur, utilisez le lien DOI ci-dessous.

Publisher's version / Version de l'éditeur:

<https://doi.org/10.1149/2.0641803jes>

Journal of The Electrochemical Society, 165, 3, pp. A547-A556, 2018-02-23

NRC Publications Record / Notice d'Archives des publications de CNRC:

<https://nrc-publications.canada.ca/eng/view/object/?id=f9d1cc25-a9cc-4fab-ad1d-840e46197a63>

<https://publications-cnrc.canada.ca/fra/voir/objet/?id=f9d1cc25-a9cc-4fab-ad1d-840e46197a63>

Access and use of this website and the material on it are subject to the Terms and Conditions set forth at

<https://nrc-publications.canada.ca/eng/copyright>

READ THESE TERMS AND CONDITIONS CAREFULLY BEFORE USING THIS WEBSITE.

L'accès à ce site Web et l'utilisation de son contenu sont assujettis aux conditions présentées dans le site

<https://publications-cnrc.canada.ca/fra/droits>

LISEZ CES CONDITIONS ATTENTIVEMENT AVANT D'UTILISER CE SITE WEB.

Questions? Contact the NRC Publications Archive team at

PublicationsArchive-ArchivesPublications@nrc-cnrc.gc.ca. If you wish to email the authors directly, please see the first page of the publication for their contact information.

Vous avez des questions? Nous pouvons vous aider. Pour communiquer directement avec un auteur, consultez la première page de la revue dans laquelle son article a été publié afin de trouver ses coordonnées. Si vous n'arrivez pas à les repérer, communiquez avec nous à PublicationsArchive-ArchivesPublications@nrc-cnrc.gc.ca.





Connection between Phase Diagram, Structure and Ion Transport in Liquid, Aqueous Electrolyte Solutions of Lithium Chloride

Chae-Ho Yim and Yaser A. Abu-Lebdeh

National Research Council of Canada, Ottawa, Ontario K1A 0R6, Canada

The nature of structure and ion transport in liquid electrolyte solutions are still not fully understood over the whole concentration range. In this work, we have studied aqueous solutions of lithium chloride as a model salt due to its very high solubility in water and ample knowledge of its structure and physicochemical properties. We have analyzed the ionic conductivity (κ) vs. concentration (C) plots based on free volume approach and our recently developed equation: $\kappa = AC \exp[-BC]$ and conductivity vs. temperature plots based on Arrhenius equation. We find that the solutions show little variation in free volume with concentration, or even temperature, but a rapid increase in activation energy and pre-exponential factor. We relate the significant changes in conductivity to changes in structure and transport in the solutions and connect them to the binary LiCl/H₂O phase diagram. We hypothesize that the changes are caused by a breakdown of the bulk water structure near the eutectic composition that causes a change in transport mechanism. We believe that this connection between solution structure, ion transport and phase diagram is common in most aqueous and non-aqueous electrolyte solutions and explains the origin of maximum in conductivity in isothermal conductivity vs. concentration plots.

© 2018 The Electrochemical Society. [DOI: 10.1149/2.0641803jes]

Manuscript submitted December 18, 2017; revised manuscript received January 26, 2018. Published February 23, 2018.

One of the most common uses of liquid electrolytes is in batteries that are becoming ubiquitous in modern society to enable electric vehicles and renewable energy sources to mitigate harmful effects of traditional energy sources on the environment. Battery electrolytes are made from moderately concentrated liquid solutions that exhibit a high ionic conductivity of 10^{-3} - 10^{-2} S cm⁻¹. This high conductivity is usually at the maximum in the isothermal conductivity vs concentration plots, to be denoted hereafter as C_{max} .¹ For example, concentrated alkaline ($C_{max} > 5$ M, KOH) aqueous solutions are used in commercial alkaline Zn/MnO₂ or Nickel Metal hydride (NMH) batteries, while concentrated acidic ($C_{max} > 6$ M, H₂SO₄) aqueous solutions are used in Lead-acid batteries. Moreover, other re-chargeable batteries with much higher operating potential such as commercial Li-ion batteries use non-aqueous electrolyte solutions made of LiPF₆ in mixed carbonate solvents at less-concentrated ($C_{max} \sim 1$ M) solutions.

Recent work on aqueous as well as non-aqueous electrolyte solutions show that there are benefits in using higher concentrations beyond C_{max} despite the drop in ionic conductivity regardless of battery chemistry:² (1) Improved rate capability of graphite and lithium metal cycling in half cells.³ (2) Inhibition of Al corrosion in common carbonate electrolytes using higher concentrations of LiTFSI.⁴ (3) Unexpected stability of lithium metal in high concentration solutions of LiTFSI in nitrile solvents or graphite in propylene carbonate, PC, or dimethylsulfoxide, DMSO.⁵⁻⁷ (4) Inhibition of metal dissolution in high voltage batteries.⁸ (5) Improved thermal stability of electrolyte solutions.² (6) Higher electrochemical stability of aqueous electrolytes (~ 3 V) to enable aqueous Li-ion rechargeable batteries.⁹

However, there is little known about the nature of structure and ion transport in liquid electrolyte solutions over the whole concentration range especially at high concentration.¹⁰ In fact, this was called the most celebrated failures in physical chemistry by Angel to demonstrate the frustration by many scientists about the lack of a model or theory that can successfully extend or replace the long-standing Debye-Hückel theory.¹¹ Moreover, the strong dependence of ionic conductivity on electrolyte concentration especially in aqueous solutions has been known for a very long time.^{12,13} This can be understood by looking closer at the structure of the solution and how it impacts transport over the whole concentration range and how it connects to the phase diagram as follows:

The structure/transport relationship.—There are two main models that try to explain the structure of the electrolyte solution and its relationship with ion transport:

1. The disordered “ionic atmosphere” model:¹

This model is based on the Debye-Hückel theory and to some extent the Gouy-Chapman theory of the electric double layer of colloids that describe the solution structure as being made of ionic atmospheres (a central ion surrounded by a diffuse layer of oppositely charged ions and solvent molecules). The transport of ions is influenced by the ionic atmosphere in two ways: relaxation effect (drag due to the asymmetry of charge distribution of a moving ionic atmosphere created by oppositely charged ions that require restructuring and this requires long “relaxation” time) and electrophoretic effect (drag due to a moving ionic atmosphere that drags solvent molecules due to ion-solvent interactions and the central ion moves in an opposite direction to the ionic atmosphere). The conductivity hence follows the Debye-Hückel-Onsager corresponding limiting law (square-root dependence of ionic conductivity on concentration) which was found empirically applicable only to very dilute concentrations (<10 mM).

An extension of the Debye-Hückel model where more effects are taken into account as concentration increases, mostly as a result of ion-dipole (solvent) interactions or ion-ion interactions, have also been proposed.¹ However, at higher concentrations (>1mM) there are strong deviations because of the collapse of the ionic atmosphere in what is known as the Kirkwood crossover.^{14,15} Many empirical, semi-empirical equations and phenomenological treatments have been proposed but all seem to endorse the idea that modeling the ionic conductivity of liquid electrolyte solutions at medium and high concentrations is a tough challenge.¹⁰ It is worth mentioning here the pioneering work of Pitzer on the strong dependence of the activity coefficient on concentration, but more so is the work of Brathel where conductivity is given by Equation 1 that can be transformed to include association constant and mean activity coefficient at high ion association also.¹⁰

$$\Lambda = \Lambda_0 - S(C)^{\frac{1}{2}} + EC \log C + J_1 C + J_2 C^{\frac{3}{2}} + \dots \quad [1]$$

2. The ordered “Loose or quasi-crystalline lattice” model:¹⁴⁻¹⁷

This model suggests that the ionic atmosphere be replaced by unit cells with fixed ions around the central ion that distribute throughout the solution and it was first proposed for molten salts. There are two aspects to this theory when it's applied to electrolyte solutions: one that combines this “ordered” model with the “random” ionic atmosphere model where the ionic atmosphere is replaced by a statistical cell and the relaxation and electrophoretic effects are adjusted. This predicts a cube-root dependence of ionic conductivity on concentration.¹⁷⁻²¹ The other is the purely ordered model where ions and solvents are distributed in unit cells and hence ion transport occurs by hopping mechanism (into vacant sites “holes”) in place of a hydrodynamic mechanism for ion transport between unit cells to emulate conductivity in defective solids (ionic solids, glass, polymer electrolytes).

⁷E-mail: Yaser.Abu-Lebdeh@nrc.gc.ca

The origin of C_{max} is explained by a transition from high-mobility to low-mobility cells. Herein, Equation 2 was introduced to describe the conductivity as related to hopping between cells that was then converted to the so-called universal equation such as the corresponding states law in Equation 3,^{22,23} introduced by Varela, Cabeza, and coworkers.¹⁵

$$\kappa = \frac{q^2 a^2}{V_\alpha k_B T} [\phi^2 \bar{v}_\alpha + (1 - \phi_\alpha) \phi_\alpha \bar{v}_\beta] \quad [2]$$

And ϕ_{max} and κ_{max} are given by:

$$\phi_{max} = \frac{\bar{v}_\beta}{2(\bar{v}_\beta - \bar{v}_\alpha)}$$

$$\kappa_{max} = \frac{q^2 a^2}{4V_\alpha k_B T} \frac{\bar{v}_\beta^2}{(\bar{v}_\beta - \bar{v}_\alpha)}$$

Where $\bar{v}_{\alpha,\beta}$ are the probability of an ion jumps in time over a barrier in α or β cells, V is ionic volume.

In the universal equation,¹⁵ all electrolyte solutions fall into one master curve when reduced conductivity, κ/κ_{max} , was plotted versus reduced concentration, C/C_{max} regardless of the type of salt or solvent used.

$$\frac{\kappa}{\kappa_{max}} = 2C/C_{max} \left(1 - \frac{C/C_{max}}{2}\right) \quad [3]$$

A similar idea was suggested by Casteel and Amis²⁴ previously, Equation 4.

$$\frac{\kappa}{\kappa_{max}} = \left(\frac{C}{C_{max}}\right)^a \exp \left[-bC_{max}^2 \left(\frac{C}{C_{max}} - 1\right)^2 - a \left(\frac{C}{C_{max}} - 1\right) \right] \quad [4]$$

Shcheredakov²⁵ compiled the conductivity data for various aqueous solutions of acids, basis, and salts at different concentrations and temperatures and found that they fit into a master curve of reduced conductivity κ/κ_{max} , versus reduced concentration C/C_{max} .

In a similar line of thought, Herlem and coworkers took into account the physicochemical properties of the salt and solvent.²⁶ They introduced a new and simple relationship to predict κ_{max} of various electrolyte solutions using the values of the dielectric constant (ϵ) and viscosity (η) of the pure solvent, and later modified it to include the effect of the strong electrolyte (salt) by taking into account its acidity/basicity following the Hard Soft Acid Base (HSAB) theory. They attributed the variation in the maxima to the differences in hardness between salt and solvent.

The ion transport/phase diagram relationship.—We have shown recently that the presence of maxima in isothermal conductivity vs. concentration plots is a common feature in both aqueous and non-aqueous liquid electrolyte solutions and some solid electrolytes.² We hypothesized that the maxima reflects a transition in the structure of the solution from model 1 of the ionic atmosphere where transport occurs by solvated ionic species diffusing long distances (along a free path) by a hydrodynamic vehicular mechanism to model 2 of the loose lattice where transport mechanism switches to a slower Grotthuss-type mechanism (ion hopping along a network -no free path).

We have also introduced the idea of connecting the structure and transport behavior of electrolyte solutions to the salt/solvent phase diagram as follows:²⁷

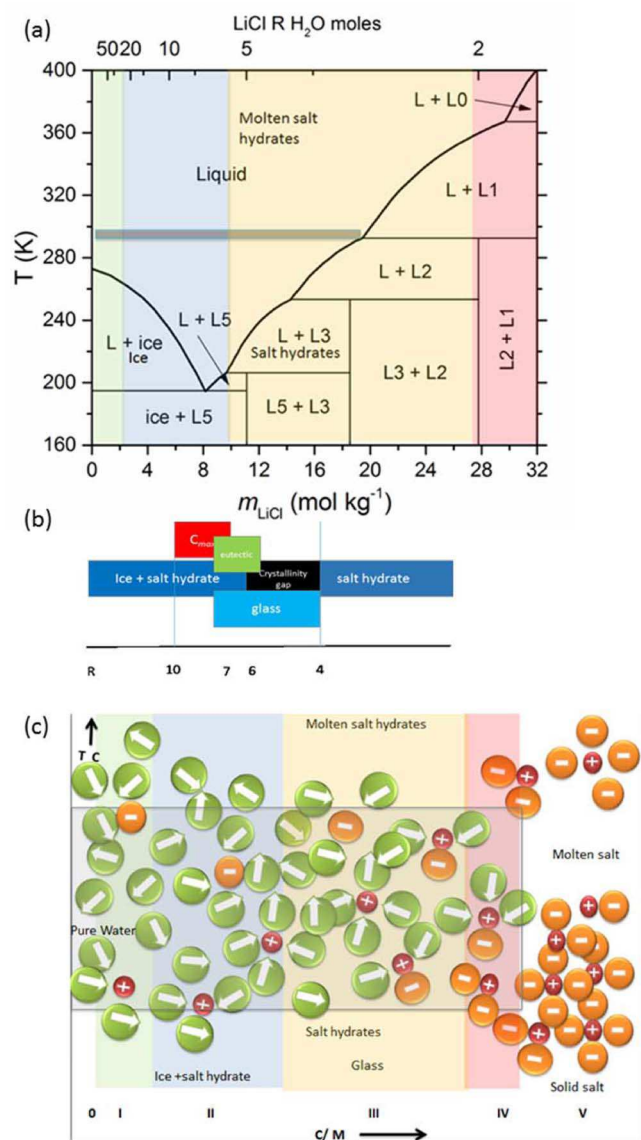
(1) Pre-eutectic concentrations, in this region the solution is dominated by hydrated ions in the case of Li salts/water being mostly $[\text{Li}(\text{H}_2\text{O})_{n=4-6}]^+$ or $[\text{Cl}(\text{H}_2\text{O})_n]^-$ in a bulk water structure that is still intact. Ion transport is believed to be due to solvated ions moving by a vehicular mechanism. In this region, ionic conductivity increases with concentration as a result of the rapid increase in the number of charge carriers that counterbalances any drop in mobility.

- (2) Near eutectic concentration, in this region the solution is very disordered, structure-less and in a state of transition (maximum entropy). Ionic conductivity does not greatly depend on the concentration and passes through a maximum.
- (3) Post-eutectic concentrations, in this region the bulk water structure breaks down and is replaced by multidimensional, dynamic structural networks made up of cations, anions and solvent molecules of the type $[\text{Li}^+(\text{H}_2\text{O})_n\text{Cl}^-]_m$. Ion transport is believed to be due to free ions moving by a Grotthuss mechanism. In this region, ionic conductivity decreases with concentration as a result of a decrease in the number of charge carriers and their mobility. Moreover, transport by Grotthuss mechanism is believed to be slower than in the vehicular mechanism due to the slow step of solvent orientation to allow for subsequent ion hops.

Moreover, regardless of the transport mechanism, ions move as a result of a gradient in Gibbs free energy in the solution. The same Gibbs free energy (ΔG°) controls the formation of the species in solution and phase transformations observed in the phase diagram. In LiCl/H₂O electrolyte solution the ΔG_f° follows the order: $\Delta G_f^\circ \text{H}_2\text{O} (-237.1 \text{ kJmol}^{-1}) > \Delta G_f^\circ \text{LiCl} (-384.0 \text{ kJmol}^{-1}) > \Delta G_f^\circ \text{LiCl.H}_2\text{O} (-631.8 \text{ kJmol}^{-1}) > \Delta G_f^\circ \text{LiCl.2H}_2\text{O} (-874.2 \text{ kJmol}^{-1}) > \Delta G_f^\circ \text{LiCl.3H}_2\text{O} (-1115.0 \text{ kJmol}^{-1}) > \Delta G_f^\circ \text{LiCl.5H}_2\text{O} (-1592.2 \text{ kJmol}^{-1})$. The excess Gibbs free energy of mixing can be calculated based on these values and of other species formed in solution and large variations in ΔG° between species will lead to faster transport.^{28,29}

The structure/phase diagram relationship.—There have been many attempts in the past to classify the structure of aqueous solutions (compositions over the liquidus lines of the phase diagram) into distinct regions over the whole concentration range from pure water to pure salt. One that has drawn our attention is the classification by Braunstein of 5 classes that were later simplified by Emmonz to 4 classes. Herein, we added two more regions: the pure water (to be called 0) and pure molten salt (to be called V) as reference points. The solution structure can then be divided into 6 distinct regions:

0. Pure solvent: There is no ion present and solvent structure is dominated by dipole-dipole interactions with no long-range order but short-range order with lots of free volume for ions to fit in. In the case of water, the structure is dominated by tetrahedrally, the hydrogen-bonded network that at low temperature freezes to various ordered structures of ice.
- I. Dilute solutions: This is the region of dilute solution where the Debye–Hückel limiting law applies in the most diluted region (0.01 *m*) and where ions are completely solvated by water. At higher concentrations ions re-arrange the solvent structure based on their charge and size (z/r^2), so introducing more short-range order around ions but the long-range order of the hydrogen-bonded network remains intact, therefore at low-temperature ice still forms along with salt hydrates.
- II. Concentrated solutions: This is the region where significant ion association takes place and extended Debye–Hückel-Onsager law applies. Again more ions introduce more short-range order locally and less long-range order in the bulk but the hydrogen-bonded network remains intact, therefore at low-temperature ice still forms along with salt hydrates. Small and large ionic species including clusters form but the solution still has enough solvent (water) molecules to keep a less dynamic but otherwise a hydrogen-bonded network intact, therefore at low-temperature ice still forms along with salt hydrates.
- III. Molten salt hydrates: Braunstein splits this region into two (III and IV in his classification). The dilute end of this region (IIIA: the hydrate melts sub-region) the number of water molecules is low but sufficient to form complete hydration shells around ions while in the second (IIIB) sub-region at the concentrated end ions do not have enough number of water molecules to form complete hydration shells. The structure is believed to



Scheme 1. a) Phase diagram of LiCl/H₂O adopted from Li et al. molar ratio R is included. L denotes a brine solution while L_r denotes the salt hydrate where r = 1, 2, 3 and 5. The colors signify the regions according to the classification. The colors signify regions of structural changes in the liquid regions. Green (I: dilute solutions), blue (II: concentrated solutions) orange (III: molten salt hydrates), Red (IV: hydrous melts); b) A schematic that highlights the most recent features between R = 4 and 10; c) A refined model for change in solution structure and transport mechanism as a function of concentration within the liquid range of the phase diagram. The gray area represents the structure at ambient temperature.

resemble that of a molten salt. This is the region where the hydrogen-bonded network breaks down and therefore ice does not form at low temperature and only salt hydrates do.

IV. Hydrous melts: this region consists of molten salt with small amounts of water. Water molecules are integrated into the lattice structure.

V. Pure salt: the solid is made up of a crystalline lattice that upon melting remains intact but becomes loose and ions become more mobile.

In order to apply such classification to the LiCl/H₂O phase diagram (LiCl·R·H₂O where R is the molar ratio), we have reconstructed the phase diagram in Schematic 1a from Li et al.³⁰ and based on the above classification overlaid a structural landscape of the short-

range order in the solutions highlighting the regions of interest at ambient temperature and the whole temperature/concentration range as shown in Figure 1b. The phase diagram exhibits a V shape that is typical of binary mixtures with a eutectic point at 8 m (R = 7) where ice, LiCl·5H₂O, and LiCl/H₂O brine coexist. It also shows four peritectic points that correspond to the formation of four salt hydrates: LiCl·H₂O, LiCl·2H₂O, LiCl·3H₂O, and LiCl·5H₂O. Also, the ice phase exists from pure water (R = 0) to 11 m (R = 5) and the glass-forming region is believed to be in the range R = 4 to R = 8 and a crystallinity gap is believed to exist between R = 4 and 6.³¹ A schematic that highlights the most critical features between R = 4 and 10 are shown in Schematic 1c.

Ion transport.—Spiro and King reviewed the transport properties of concentrated aqueous electrolyte solutions up until the late seventies and commented that neither the ionic atmosphere model nor the lattice model describes well the transport behavior in concentrated solutions.³² Instead, they argued that the most applicable approach is the transition state theory. The transport process is in this regard an activated process and ions need to come over an energy barrier regardless of the type of order in the structure. In this regard, the most relevant is the work by Angell and Bressel¹¹ who used the statistical thermodynamic approach of Adam and Gibbs to transform the Vogel-Tammann-Fulcher empirical equation that describes temperature dependence of conductivity (transport properties in general) to an isothermal concentration dependence one, Equation 5.

They assumed a linear dependence of the ideal glass transition temperature, T₀, on concentration. A and B are constants. They verified the results experimentally by fitting the data to Equation 5 for aqueous solutions of Ca(NO₃)₂ over a wide range of concentrations and temperatures.

$$\kappa = X \frac{A'}{\sqrt{T}} \exp\left(\frac{-B'}{X_0 - X}\right) \quad [5]$$

Where X is the molar ratio of the salt, X₀ is the molar ratio at T₀. Unfortunately, information about X₀ for many solutions is not available and the dependence of T₀ on X is not in many cases linear especially at extreme compositions as suggested by the authors themselves.

Recently, the original ideas of Doolittle and Cohen-Turnbull on free volume have been applied by Krause-Rehberg and coworkers to ionic liquid electrolytes and our research group to molecular liquid electrolytes and new relationships that correlate transport to free volume have been introduced.^{27,33} They introduced an equation to correlate the viscosity and ionic conductivity of neat ionic liquids at different temperatures to free volume. While our research group measured the ionic conductivity (κ) of lithium and other alkali metal salts in aqueous and non-aqueous electrolyte solutions as a function of concentration (C) and fitted them to Equation 6. This is a new, isothermal, semi-empirical equation based on free volume introduced by our research group following a similar line of thought to that of Angell and Bressel's and Equation 5.¹¹ First, we related B to a term that has free-volume dependence ($\frac{V_f^*}{V_f}$). Then C, molar concentration, was introduced in the pre-exponential and exponential terms similar to Equation 5.

$$\kappa = AC \exp[-BC] \quad \text{or} \quad \Lambda = A \exp[-BC] \quad [6]$$

Where

$$B = \frac{\gamma V_o}{V_f}$$

V_f is the free volume which can simply be defined by the difference between the measured volume of the liquid (from density measurements) and the occupied volume, V_o. V_o is simply the minimum occupied volume (closely related to Van der Waals' molecular volume) by the molecules and is temperature independent, i.e. the volume at absolute zero. There is uncertainty in obtaining accurate values of V_o but it can be estimated by X-ray diffraction techniques or else be calculated using computational methods. A and B are

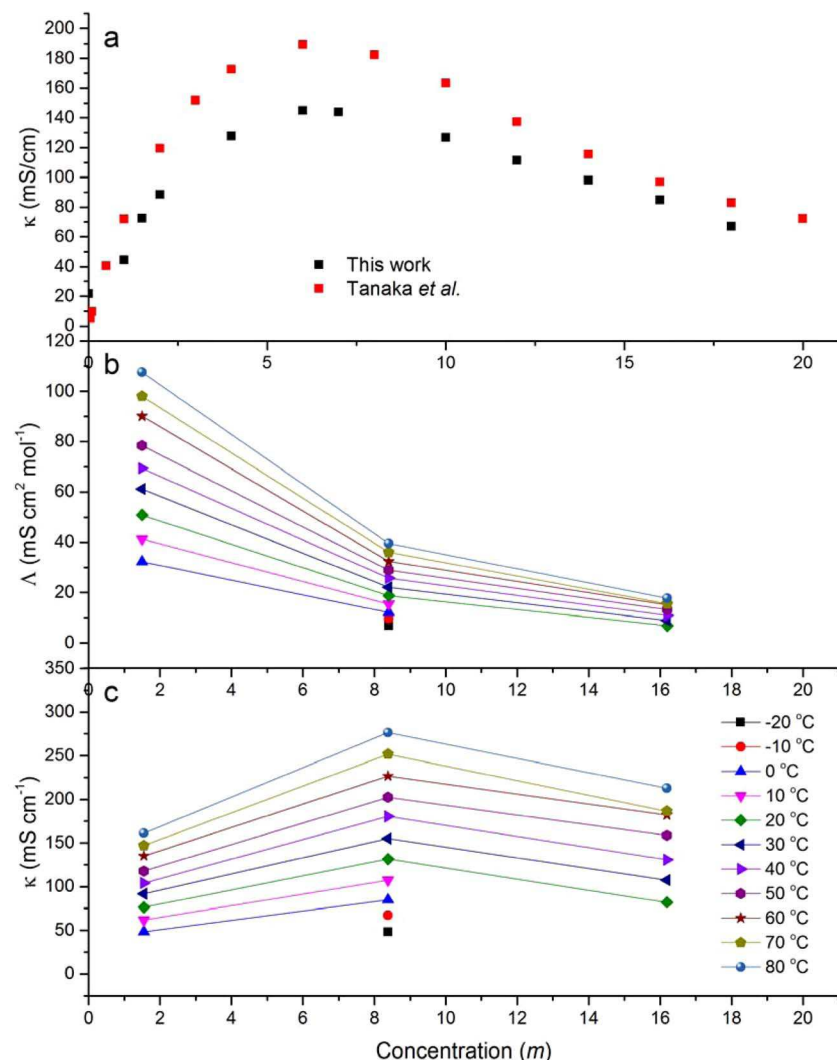


Figure 1. (a) ionic conductivity, κ , of LiCl aqueous solutions as a function of concentration at 25°C measured in this work and adopted from Tanaka et al. (b) molar ionic conductivity (Λ) of the three selected concentrations as a function of concentration. (c) ionic conductivity (κ) of the three selected solutions as a function of temperature.

parameters that could be related to charge carriers and activation energy of transport, respectively.

We previously have investigated mostly non-aqueous solutions and few aqueous solutions but not over the whole concentration range.²⁷ Therefore, in this work, we have investigated the conductivity of aqueous solutions of lithium chloride, LiCl, as a model salt because of its very high solubility in water that allowed us to study the high concentration region up to saturation at 20 m . We have analyzed the data using Arrhenius plots and calculated activation energies and pre-exponential factors that strongly depend on concentration especially after C_{max} or the eutectic composition in the LiCl/H₂O phase diagram. We calculated the free volume for each concentration at each temperature from measured densities and analyzed the data using the free-volume approach and the newly developed equation.

Experimental

The solutions with molality (m) between 1.5 m and 18 m were prepared by dissolving known amounts of LiCl (Aldrich) in de-ionized water and left to equilibrate overnight. Density measurements were carried out using a DMA 35 (portable density meter from Anton Paar). The estimated errors are 0.001 g/ml . Conductivity measurements were carried out using conductivity meter RL060C from Thermo Scientific equipped with a water bath to control the temperature between 20°C and 80°C . The estimated errors are 1% . In some cases, conductivity measurements were carried out using AC impedance spectra. The frequency range was 1 $\text{kHz} - 1$ Hz swept using a Solartron frequency

response analyzer (FRA) 1255B coupled with a Princeton Applied Research (PAR) 263A potentiostat. The electrolyte was poured into a two-platinum-electrode conductivity cell ($K = 1$ cm^{-1}).

Results and Discussion

Ionic conductivity of electrolyte solutions as a function of salt concentration and temperature.—The ionic conductivity of the aqueous electrolyte solutions of LiCl was measured over the whole concentration range up to saturation at room temperature, 293 K and also in the temperature range $273 - 353$ K .

Figure 1a shows a plot of the specific ionic conductivity, κ , versus molal concentration (m) at 398 K along with the literature values obtained from Tanaka et al.³⁴ The figure has a typical bell shape with an increase in conductivity at low concentration, reaching a maximum at intermediate concentrations (6 m), a decrease at a higher concentration reaching saturation at 20 m . Our values compare well with the reference values except in the mid-range region where our values are lower; the maximum in conductivity ($\kappa_{max} \sim 160$ mS/cm) is lower than the value at ~ 190 mS/cm from Tanaka et al. but higher than the value ($\kappa_{max} \sim 140$ mS/cm) reported by Prasad et al.³⁵ The variations could be due to differences in solution preparation, type of cell and testing method. We used the AC impedance method to calculate the conductivity from the resistance obtained from the frequency independent region of the spectra. This is more accurate than commonly used methods where values are based on a single frequency (10 kHz) measurement in commercial conductivity meters.

κ_{max} takes place at a certain concentration, C_{max} , and has been given some significance by many researchers in the past and our research group very recently.^{24,27,34} We have hypothesized that C_{max} might represent a change in transport mechanism as a result in a change in the structure of the electrolyte solution which takes place near the eutectic region (8 m , $R = 7$) of the LiCl/H₂O phase diagram. We can, therefore, split the plot into three distinct regions:

- (1) Below C_{max} (6 m , $R = 9$): The conductivity of the solutions increases linearly with concentration up to 5 m ($R = 10$) where thereafter it increases slowly to reach C_{max} . Solutions in this region represent region I and II in the classification and compositions pre eutectic point in the phase diagram that shows LiCl·5H₂O salt hydrate and ice at low temperature (<190 K).
- (2) Near C_{max} (6 m , $R = 9$): The conductivity of the solutions does not vary greatly with concentration and extends as a bottom of a bell between 5–8 m ($R: 10-7$). Solutions in this region represent regions II and III A in the classification or compositions near eutectic point 8 m ($R = 7$). This corresponds to LiCl·5H₂O salt hydrate and ice at the eutectic temperature (<190 K) in the phase diagram. This coincides with the glass forming region between $R = 8$ and 4 which indicates a higher disorder in the bulk solution that takes place near the eutectic composition leading to no defined chemical composition. This could resemble the situation in metallic glass and supercooled liquids that near eutectic composition show the local short-range order of structurally frustrated icosahedral units that might have been inherited from similar structural units (cybotactic groups) of the liquid to help minimize interactions between metal solute and solvent molecules and lead to stabilization of the eutectic.³⁶⁻³⁸ H. Tanaka showed that this situation can be applied to LiCl/H₂O mixtures where the effect of the salt resembles that of pressure and leads to a breakdown of the hydrogen-bonded tetrahedral bulk structure of water.³⁹ We can add that the formation of pentahydrate and not a tetrahydrate might support the existence of five-fold asymmetric structures in solution.⁴⁰ However, a very dynamic equilibrium between LiCl·4H₂O and LiCl·6H₂O could exist with one water molecule hopping in between the two structures and in the solid the unit cell of the pentahydrate salt could be made of the tetrahydrate salt and an extra "loose" water molecule. Also, pentahydrate could represent the basic structural unit similar to the 13-atom icosahedron known to exist in metallic glass but in this case it could consist of 14 ions and water molecules to maintain neutrality. An example of such units is [Li(H₂O)₅ Cl(H₂O)₅ Li]⁺Cl⁻ or [Cl(H₂O)₅ Li(H₂O)₅ Cl]⁻Li⁺.⁴⁰
- (3) After C_{max} (6 m , $R = 9$): Solutions in this region represent regions IIIB or compositions post a eutectic point in the phase diagram. The conductivity of the solutions decreases linearly with concentration above (8 m , $R = 7$) and stagnate close to saturation. This corresponds to LiCl·3H₂O and LiCl·5H₂O salt hydrates at low temperature (<200 K) in the phase diagram.

Figures 1b and 1c show the specific ionic conductivity Λ (κ/C) and ionic conductivity of three solutions that represent the whole concentration range: before C_{max} (1.5 m), near C_{max} (8 m) and after C_{max} (16 m) as a function of temperature. The plots of Λ vs. C show an expected decrease in the specific molar conductivity with concentration for all the solutions with conductivity converges at a constant value at the highest concentration at 0.4 mS/cm (extrapolated and from values for the 20 m solution). The plots of κ vs. C follow the same Gaussian-type trend over the whole temperature range.

In order to obtain the activation energy for each solution, Arrhenius plots were constructed for the data from Tanaka et al. as shown in Figure 2. We then calculated the activation energy for each solution and plotted them as a function of concentration as shown in Figure 3a. The activation energies were found to lie in the range 13 – 20 KJ mol⁻¹ for all solutions and show an interesting behavior where activation energy goes through a minimum near C_{max} and the eutectic composition then increases significantly beyond 10 m ($R = 5.5$). The

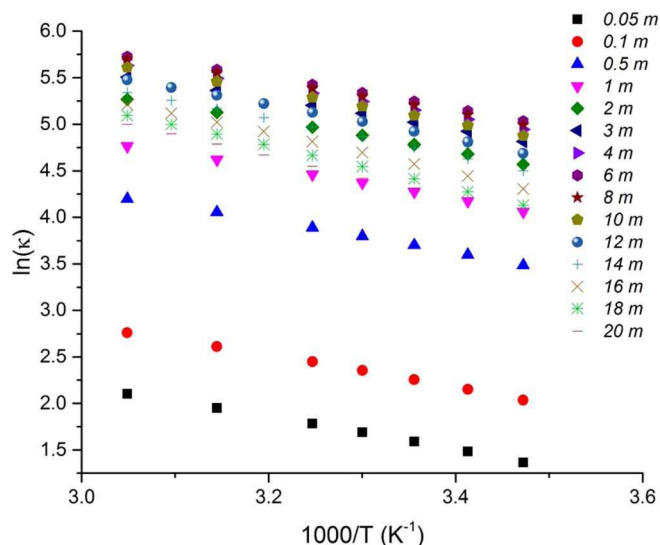


Figure 2. Ionic conductivity, $\ln(\kappa)$, of LiCl aqueous solutions as a function of temperature (T).

activation energy is higher for the most concentrated solutions reflecting the strong coulombic interactions among ions and between ions and dipoles. Tanaka et al. showed a similar trend with activation energies obtained from viscosity measurements increasing significantly after 6 m and then more significantly at 10–12 m .³⁴

We then plotted the activation energy (from Figure 2) vs. the four-third-root of concentration according to Equation 7 as shown in Figure 3b.

$$E_{a,A} = E_{a,A}^{\circ} + \frac{2(N_{AV})^{\frac{4}{3}} e^2 M V_m}{4\pi\epsilon^{\circ}\epsilon_1 Z^{\frac{1}{3}}} C^{\frac{4}{3}} \quad [7]$$

Where $E_{a,A}^{\circ}$ is the activation energy for the conductivity at very dilute concentration, M is a Madelung-like constant (1.74 is often used for FCC lattice), Z is the number of ions in a unit cell (4 for an FCC lattice), $e = 1.6 \times 10^{-19}C$, ϵ_r is the static dielectric constant of the solvent, $\epsilon_0 = 8.82 \times 10^{-12} Fm^{-1}$, and N_{AV} is Avogadro's number.⁴¹ This kind of dependence implies that the structure is close to a quasi-lattice where dipole-dipole interaction has no significance and the solution is dominated by ion-ion and ion-dipole interactions. Chagnes et al. found a fair agreement between experimental and theoretical activation energy in non-aqueous electrolytes of γ -butyrolactone with different salts, but still within limited concentration range <2 M.⁴¹ Clearly, the activation energies of the non-aqueous solutions are lower than those of LiCl/H₂O and range between 10 and 15 KJ mol⁻¹ but herein we clearly do not see any linear dependence.

The intercept of Figure 2, or the pre-exponential factor, was obtained and it also plotted versus concentration as shown in Figure 3c. It shows an increase up until 5 m ($R = 10$) then stagnates to increase again at 10 m ($R = 5.5$). Tanaka et al. did not plot the pre-exponential factor from conductivity data but from viscosity data and showed that $\ln A$ increases with concentration and drops at 12 m and then stagnates. So we can summarize that both activation energy and pre-exponential factor increase significantly at high concentrations and might be responsible for the drop in conductivity at high concentrations beyond C_{max} and eutectic composition (8 m , $R = 7$). This sharp increase in the two values of activation energy and pre-exponential factor at high concentrations resembles the behavior in molten salts at high temperatures. Aravindakshan et al. studied the origin of electrical conductivity maxima of molten salts as a function of temperature for molecular liquids (HgBr₂) and covalent network liquids (SnCl₂, PbCl₂, BiCl₃).³⁷ They in both cases showed by simulation the existence of a bromide-exchanged or chloride-bridged Grotthuss chain similar to aqueous solutions of acids and bases where ions (H⁺, OH⁻)

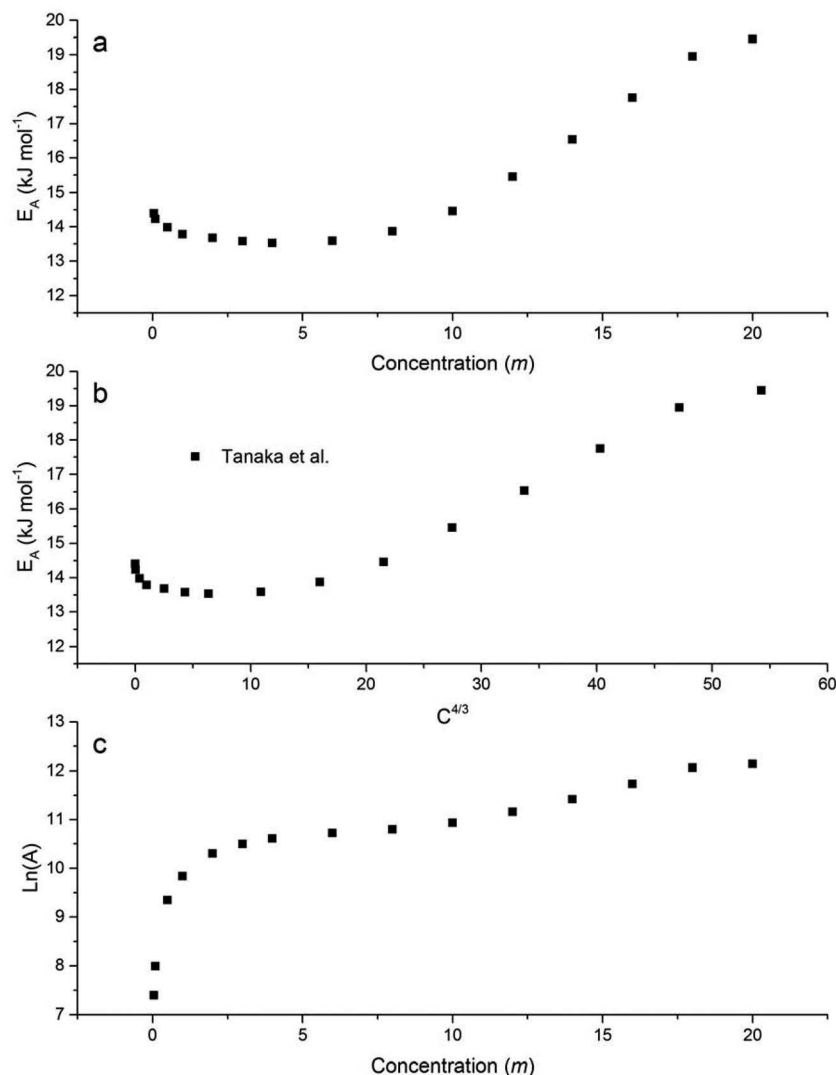


Figure 3. (a) activation energy for all LiCl aqueous solution as a function of concentration, (b) activation energy for all LiCl aqueous solution as a function of the four-third root of concentration, (c) Pre-exponential factor for all LiCl aqueous solution as a function of concentration.

can hop along the chain. Next, they attributed the drop in conductivity at a higher temperature to a rise in activation energy in network liquids and to a drop in a pre-exponential factor for molecular liquids and not to a simple ion association. Herein, a similar situation can be envisaged in the case of LiCl/H₂O where the 3D, hydrogen-bonded network is replaced by chains of chloride, Li cation, and water. Hence, the ion-ion and ion-dipole interactions decrease the “hopping” collision frequencies causing a drop in pre-exponential factor and increase the barrier for ions to escape their site “cage” causing an increase in activation energy.

More on the structure of LiCl/H₂O solutions.—There are not many studies on the structure of electrolyte solutions over the whole concentration range. X-ray and neutron diffraction along with spectroscopic studies are available for a limited number of solutions. X-ray diffraction studies of aqueous solutions compared to pure water showed that the halo (broad peak) of the bulk ordered water structure tend to disappear beyond the concentration that corresponds to the eutectic composition and the appearance of weak peaks that might be attributed to structural units, cytotactic groups, that form precursors for salt hydrates at low temperature.⁴² However, for LiCl/H₂O solutions the situation is slightly different as more in-depth studies exist due to the interest in extrapolating the information from the structure of the eutectic concentrations at low temperature to bypass the no-man’s land region that precludes the understanding of the water structure

at low temperature. Singh et al. studied structure and diffusivity of aqueous LiCl solutions in the entire range by molecular dynamics (MD) simulations and found a strong solvation of monovalent ions in water and cluster formation at higher salt concentrations.⁴³ The diffusion coefficient of LiCl was found to decrease depending on the coordination number and geometry that change with the salt concentration. Aouizerat-Elarby et al. also studied the structure and diffusion in LiCl solutions over the whole concentration range.⁴⁴ They showed that in the range $0 < R < 3$ the solution is predominantly ionic in nature. For R values close to 6 and 4, there is no defined compound and deep eutectics are formed. Their structural analysis showed a complete hydration sphere for $R = 6$ and a direct anion-cation interaction for $R = 4$. This explained the diffusion coefficient values for Li, Cl, and water that were similar above $R = 100$ where water structure is still intact. This changes around $R = 90$ to 100 where chloride ions modify the structure and again different values occur at $R = 3$ and $R = 12$ indicating dependence on the presence of chloride in the first or second solvation shell.⁴⁴ In a very recent work, Prasad et al. studied the structural and dynamic changes and thermodynamic properties of aqueous LiCl solutions over the whole range and connected them to the experimental phase diagram. They observed by MD simulation the breakdown of the hydrogen-bonded network of water as the LiCl concentration crosses the eutectic composition and they showed pronounced monotonic decrease in diffusivities of H₂O, Li⁺ and Cl⁻, accompanied by an increase in viscosity.³⁵ They also compared the structural asymmetries of H₂O (tetrahedral) and LiCl

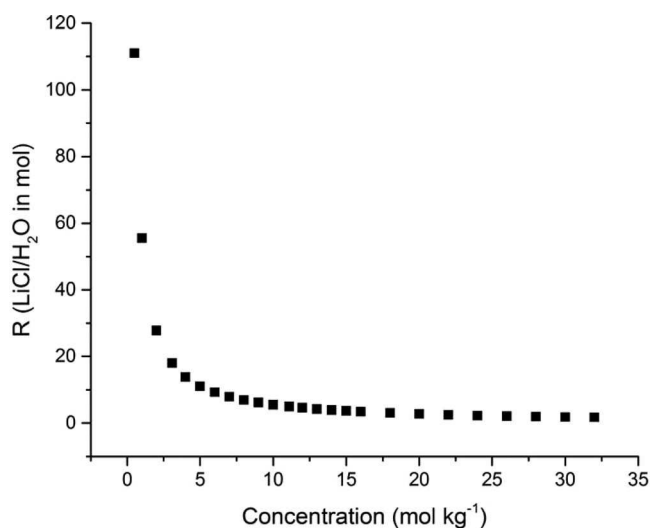


Figure 4. Variation of the LiCl/H₂O molar ratio, R, with concentration.

(cubic) to that of BeF₂ (tetrahedral) and LiF (cubic) and suspected a breakdown of the tetrahedral structure as the origin of the V-shape of the binary phase diagram. Green et al. studied the Raman scattering of LiCl/H₂O solutions between 5 to 15 mol% LiCl ($R = 6.6$ to 20) and found that a coordination number of 5.5 dominates in this range and at different temperatures and concluded that the addition of LiCl to water breaks the hydrogen bonded tetrahedral structure.⁴⁵ Finally, it is worth looking at the molten LiCl to get more insight on structure and transport. McGreevy and Howe showed by neutron scattering that the structure of molten LiCl retains the octahedral symmetry of its solid FCC structure with the small lithium cation being coordinated by an octahedron of six of the larger Cl⁻ anions with at least one vacant site, rather than a tetrahedron due to the very large charge density of Li⁺.⁴⁶ It follows that the conductivity mechanism in the liquid “molten” salt might be similar to that in the solid where ions conduct by the widely accepted Schottky (vacancy-assisted ion hopping) mechanism. The primary charge carrier in the molten salts is the cation with reported transport numbers higher than 0.9 where chloride ions form the backbone of a semi-lattice similar to the solid. The conductivity of molten LiCl at > 900 K is 5.6923 S cm⁻¹ and the activation energy is 6.3 KJ mol⁻¹ while the pre-exponential factor (frequency factor) is 13 S cm⁻¹.⁴⁶ Moreover, we used the data from Reference 43 in order to calculate the specific ion conductivity of the molten LiCl from reported densities and conductivities of the melt at different temperatures. The specific ion conductivity of the molten LiCl was found to be $\Lambda^{\circ}_{\text{LiCl}} = 161.2 \text{ S cm}^2 \text{ mol}^{-1}$ ⁴⁷ at 893 K and increasing to 198.5 S cm² mol⁻¹ at 973 K. The values are not very much higher than the one in dilute solutions, $\Lambda^{\circ}_{\text{LiCl}} = 115.03 \text{ S cm}^2 \text{ mol}^{-1}$, that might indicate that conductivity mechanisms in both extreme ends of the concentration range despite the latter being at a very high temperature (>870 K) might be of similar nature.

To summarize, it is clear that the solution goes through changes in its short-range order and long-range order as a function of LiCl concentration or R. To emphasize the point, we plotted R versus concentration as shown in Figure 4. It clearly shows that there is a dramatic drop in the number of water molecules per mole of LiCl as the concentration approaches 5 *m*. At lower concentrations there are plenty of water molecules, for example at 0.5 *m* there are 110 molecules of water for every LiCl that drops to 55 at 1 *m*. At concentrations beyond 5 *m* it is less than 10 molecules of water which hardly sufficient to solvate both the lithium cation and the chloride anion as will be described below. If we focus on the short-range order in the vicinity of the ions⁴⁸ then there seems to be critical R values 3, 7, 12 and 24 which corresponds to concentrations 18, 8, 5, 2.5 *m* respectively, that cause structural changes as follows:

1. In dilute solutions of region I, the small Li ions fit into the plenty of free volume available in the tetrahedral bulk structure of water and re-arrange water molecules around them forming solvated ions with full first (6 H₂O molecules) and second (12 H₂O molecules) solvation shells, [Li(H₂O)₆(H₂O)₁₂]⁺ whereas the bigger chloride anion is known to be loosely solvated with less number of water molecules [Cl(H₂O)_{*n*<6}]⁻. This corresponds to $R \geq 24$; $m = 2.5$ region where the conductivity increases as the number of charge carriers increases.
2. In concentrated solutions of region II, the number of water molecules drop in the first shell to 4 and in the second solvation shell to below 8 [Li(H₂O)₄(H₂O)_{<8}]⁺. and Cl anions are less and less solvated [Cl(H₂O)_{*n*<6}]⁻ and the tetrahedral bulk structure of water is still intact. If we assume 4 molecules in the second solvation shell and 4 for the chloride, then $R = 12$; $m \sim 5$. This is when the conductivity dependence switches from linear to curved and signifies the onset of the C_{max} region. The conductivity increases as the number of charge carriers increases and their mobility as a result of lower number of water molecules in the solvation shells.
3. In the diluted end of region IIIA the number of water molecules in the first shell remains 4 but drops to below 4 in the second solvation shell [Li(H₂O)₄(H₂O)_{<4}]⁺ and possibly when the chloride anion enters the second solvation shell [Li⁺(H₂O)₄(H₂O)₃Cl⁻]. If we assume chloride anion is not solvated then $R = 7$; $m = 8$ and that is the eutectic point. This is when the most significant change in structure takes place and leads to the breakdown of the tetrahedral bulk structure and formation of structural units such as the icosahedrons that stabilize the liquid and lead to a deep eutectic. In the concentrated end of region IIIB the second shell disappears and number of water molecules drop to below 4 and the chloride ion enters the first solvation shell: [Li⁺(H₂O)₃Cl⁻], then $R = 3$; $m \sim 18$. The conductivity in this region drops due to the decrease in the number of charge carriers and or their mobility by a Grothuss-type mechanism along the structure that is dominated by multi-dimensional networks of the type [Li⁺(H₂O)₃Cl⁻]_{*y*}.

It seems that so long as the chloride ions do not enter the second coordination shell of lithium ions the solution tetrahedral structure remains intact and transport is vehicular and conductivity increases with concentration. As it enters the second shell ($R < 11$) the ions become closer to each other and start feeling their electrical fields very strongly and herein the conductivity starts to stagnate, approaches C_{max} and when it enters the first shell ($R < 3$) the conductivity decreases. However, the liquid state is very dynamic and water molecules exchange position around the ion and the bulk very rapidly with residence time in 10⁻¹² s. Also, ion association and even the formation of inhomogeneous, nano-sized clusters of LiCl over the whole concentration range has been reported.⁴⁹ It is also worth mentioning that, other conductivity mechanisms were proposed where H₃O⁺ or OH⁻ ions could be responsible for conductivity while dissociated ions of the salt and water are passive and work as a substrate.⁵⁰ Another conductivity mechanism is the string-like ionic movement where ions hop between lattice sites⁵¹ while diffusion is constrained. For example, lithium ion hopping between tetrahedral sites in antiferroite Li₂O, or other superionic conductors enter a jamming state that can resemble structures that cause the C_{max} .⁵²

In order to show the significance of C_{max} and κ_{max} , we plotted reduced conductivity, κ / κ_{max} , vs. reduced concentration, C / C_{max} , for all the solutions at different temperatures as shown in Fig. 5a. It can be seen all the data fitted into one master curve that slightly diverges at the higher end of the concentration range. Next, we plotted Λ / Λ_{max} vs. C / C_{max} and the plot showed a similar trend to Λ vs. C curve as shown in Fig. 5b. Then, we linearized it by plotting $\ln(\Lambda / \Lambda_{max})$ vs. C / C_{max} as shown in Fig. 5c. The plot was linear with 0.99 regression and fits well Equation 8. The obtained average values for *a* and *b* were 2.77 and 1, respectively:

$$\frac{\Lambda}{\Lambda_{max}} = a \exp(b C / C_{max}) \quad [8]$$

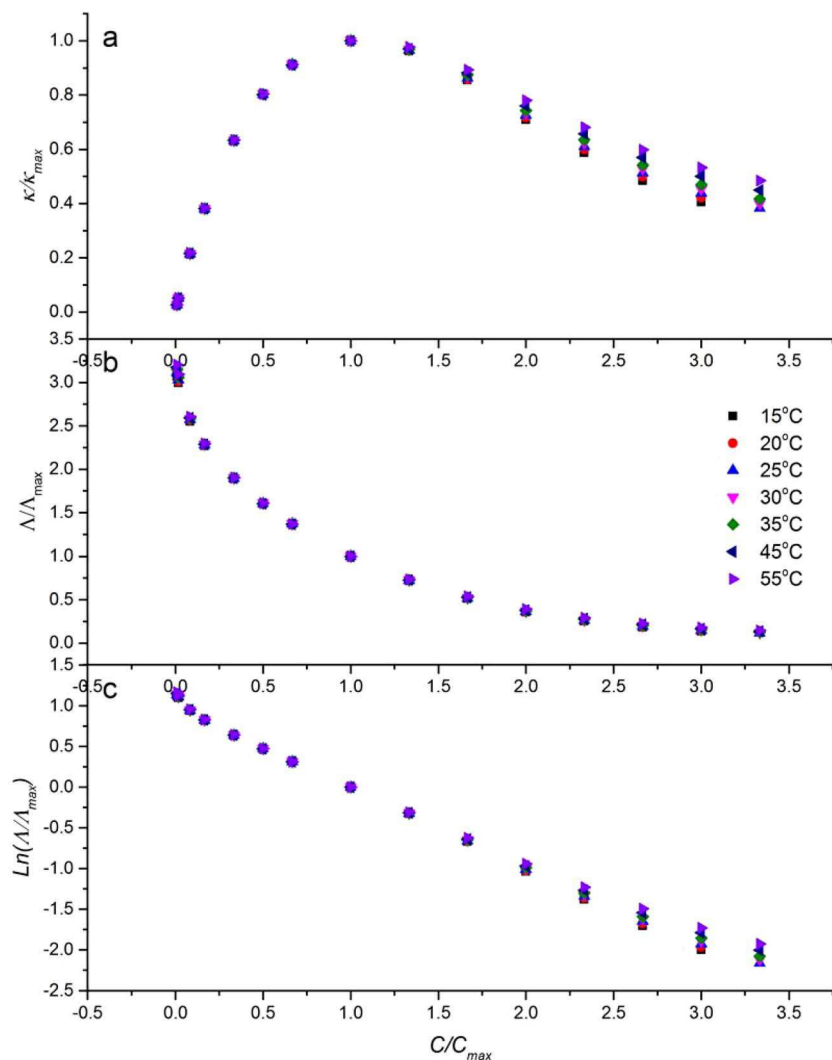


Figure 5. Plots of a) reduced conductivity κ/κ_{max} , b) specific conductivity Λ/Λ_{max} and c) $\ln(\Lambda/\Lambda_{max})$ as a function of reduced concentration C/C_{max} for all the solutions at different temperatures.

This is quite similar to the two-parameter Casteel-Amis equation, Equation 4, and the corresponding states law, mentioned in the introduction.²⁴ The significance and physical meanings of a and b parameters is still not known and Casteel and Amis suggested treating them as constants that are characteristic of each salt/solvent system. However, we are currently investigating the meaning of the two parameters in the equation.

Fitting of ionic conductivity based on the free volume approach.—The free volume, V_f , was calculated for each solution from the density as described in details in our previous publication but briefly by:²⁷

$$V_f = V_b - V_o$$

Where V_b is the volume of the liquid calculated for each solution from density measurements and V_o is the occupied volume, or simply Van der Waals' molecular volume of the LiCl and water molecules. The calculated free volume of the solutions as a function of concentrations at room temperature are shown in Figure 6 along with calculated free volume from density values from Tanaka et al.^{27,34} In general, it can be seen that the free volume decreased steadily with concentration from 11.5 ml mol⁻¹ for pure water down until the saturated solution reaching ~10 ml mol⁻¹. The plot also shows variation in free volume as a function of temperature and the decrease is even less significant and it was only 0.5 ml over the whole temperature range. The results indicate that even at the highest concentration there still exist plenty of free volumes in the solution and there are no abrupt

changes around the C_{max} or near eutectic composition. However, we have previously decomposed the volume of the solution into its components and showed that the free volume calculated herein represents the total free volume that is accessible and inaccessible for the ions

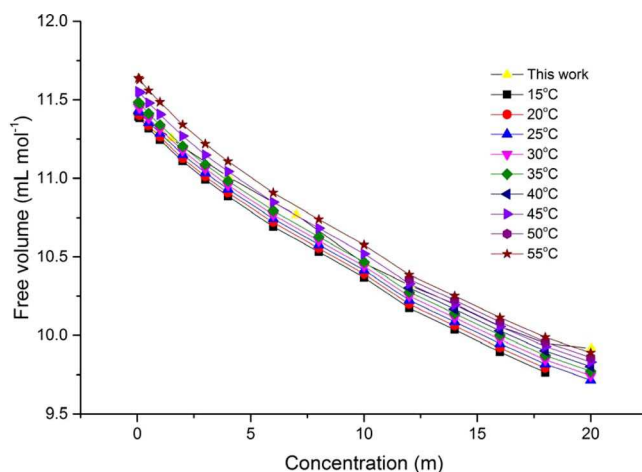


Figure 6. Free volume for all LiCl aqueous solution as a function of concentration calculated from density measurements.

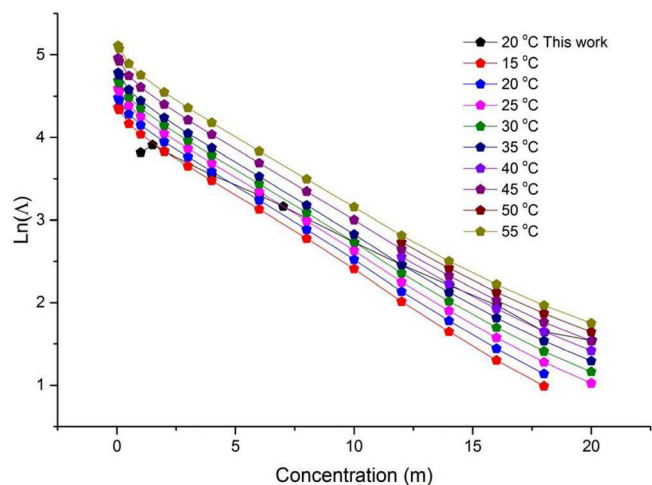


Figure 7. Logarithms of specific ionic conductivity, $\ln(\Lambda)$, measured in this work and adopted from Tanaka et al., of LiCl aqueous solutions as a function of concentration and temperature.

and water molecules to diffuse²⁷ and there might be changes in the ratio of the two that is very hard to decouple.

In order to correlate the free volume to conductivity, we previously showed that plots of $\ln \Lambda$ vs. C and plots of $\ln \Lambda$ vs. V_o/V_f (inverse of fractional free volume) for many aqueous and non-aqueous solutions are not linear especially at high concentrations but plots of $\ln \Lambda$ vs. $C \cdot V_o/V_f$ (the product of concentration and inverse of fractional volume) are linear.²⁷ However, herein, Figure 7 shows plots of $\ln \Lambda$ vs. C for all LiCl aqueous solutions are reasonably linear over the studied range of concentrations and temperatures.

The data were fitted to Equation 6 and the obtained average value for the slope (B) is 0.164. If we assume V_f is a constant with an average value of 10 ml mol⁻¹ and V_o is 23 ml mol⁻¹, then γ is 0.07. This value is way out of the theoretical range of 0.5 and 1. We have shown previously that the γ values for the non-aqueous solutions fell within what is typically obtained for ionically conducting amorphous materials such as glass, polymer electrolytes, and ionic liquids⁵³ while the low values for aqueous solutions are outside the theoretical limits. Out-of-range values have been reported for aqueous solutions of LiTFSI by our research group and ionic liquid electrolytes by others.^{27,33,54} In this case even though it might indicate a great interaction/free volume overlap, other parameters possibly energy contribution such as volume activation energy might come into play and hence the slope does not represent γ alone as a correlation factor for free volume overlap. Also, herein V_o is variable because it is the sum of $V_{o, \text{solvent}}$ and $V_{o, \text{salt}}$, where $V_{o, \text{solvent}}$ is assumed to be constant while $V_{o, \text{salt}}$ increases as salt are added. This is different from temperature dependence measurements of conductivity where the slope is a constant and is correlated to the molecular volume of monomeric repeating units of guest polymers in polymer electrolytes or molecular size of the ionic liquid, V_{conduc}^* .⁵⁴ Also, V_f is actually changing as shown above by 17.5% over the whole concentration range, so both should be treated as variables. Therefore, we, similar to our previous work, plotted $\ln \Lambda$ vs. $C \cdot V_o/V_f$, and results are shown in Figure 8. The value for the slope γ is 0.23 at room temperature which is closer to the theoretical value than the one obtained from the $\ln \Lambda$ vs. C plot.

The room temperature value for the intercept, $\ln A$, is 4.46 S cm² mol⁻¹ from the $\ln \Lambda$ vs. $C \cdot V_o/V_f$ plot and 4.7 cm² mol⁻¹ from the $\ln \Lambda$ vs. C plot which corresponds to A values of 73 S cm² mol⁻¹ and 109.9 S cm² mol⁻¹, respectively. The significance of A is not obvious in the isothermal equation as pointed out by Cowie et al. in the case of polymer electrolytes⁵⁵ but we have shown that in certain liquid solutions it could be related to the specific molar conductivity (Λ°).²⁷ The values are close to the known value for dilute LiCl solution at

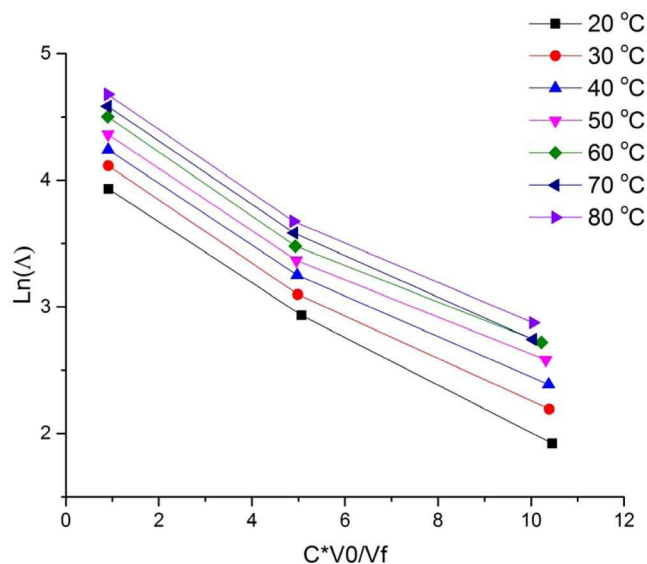


Figure 8. Plot of $\ln \Lambda$ vs. CV_o/V_f (inverse of fractional volume) for all solutions for the three selected concentrations.

25 °C, $\Lambda^\circ_{\text{LiCl}}$, 115.03 S cm² mol⁻¹,⁴⁷ and in the melt $\Lambda^\circ_{\text{LiCl}}$, 161.2 S cm² mol⁻¹, as calculated above.

We are currently looking into other ways to interpret B. One of the approaches is to treat B as a ratio between electrical energy (coulombic forces as a result of ion-ion and ion-dipole interactions) to thermal energy (RT , ~ 2.5 KJ mol⁻¹ at 25 °C) that is a constant in our isothermal plots. This will incorporate the dielectric constant (ϵ) into the equation. It is known that the dielectric constant drops with concentration and others have attempted to include a ϵ dependence on the pre-exponential factor and corrected the Arrhenius equations but only for dilute liquid non-aqueous solutions.⁵⁶

Conclusions

In this work, we have studied the ionic conductivity of LiCl aqueous solutions over the whole concentration range and fitted the data to our recently developed semi-empirical equation based on the free-volume approach. We concluded the following:

1. The ionic conductivity of the LiCl/H₂O solutions shows a maximum at the concentration, C_{max} that coincides with the eutectic region in the phase diagram.
2. The activation energy was calculated from the Arrhenius plots and showed a minimum around C_{max} and near the eutectic composition and increased significantly thereafter. This was interpreted as the cause of the maximum.
3. The free volume, calculated from measured density for each electrolyte solution, decreased insignificantly with concentration over the whole concentration range by about 2 ml and with temperature by only 0.5 ml. Free volume and conductivity data were fitted to the newly developed equation and correlation between conductivity and free volume still not fully clear. The free volume was correlated to conductivity using equation 11 and plots of $\ln \Lambda$ vs. $C \cdot V_o/V_f$ but the significance of the slope and intercept are still not clear.
4. We showed that the structure and transport of the LiCl/H₂O solutions can be connected to the binary phase diagram in many ways: First, the C_{max} in the conductivity vs concentration plot coincides with the near eutectic composition and signifies a transition in solution structure and transport caused by chloride anions entering the second solvation shells of lithium cations. Second, the formation of ice at low temperature that extends to a composition just beyond the eutectic can be taken as an indirect evidence for the breakdown of the bulk water structure into multidimensional

networks of chloride, lithium ions and water that causes a change in conduction mechanism from the vehicular mechanism of solvated ions to the slower Grotthuss-type mechanism of naked ions hopping along the network.

- Concentrated LiCl/H₂O electrolyte solutions have the potential to support electrochemical activity at high potentials due to the immobilization free water molecules preventing their decomposition to H₂ and O₂ gases.

Acknowledgment

The authors thank Natural Resources Canada for partial financial support through the Program for Energy Research and Development (PERD) and Energy Innovation Program (EIP).

ORCID

Yaser A. Abu-Lebdeh  <https://orcid.org/0000-0001-8936-4238>

References

- D. Aurbach, *Nonaqueous electrochemistry*, CRC Press, 1999.
- Y. Yamada and A. Yamada, *Journal of The Electrochemical Society*, **162**, A2406 (2015).
- Y. Yamada, M. Yaegashi, T. Abe, and A. Yamada, *Chemical Communications*, **49**, 11194 (2013).
- D. W. McOwen, D. M. Seo, O. Borodin, J. Vatamanu, P. D. Boyle, and W. A. Henderson, *Energy & Environmental Science*, **7**, 416 (2014).
- Y. Yamada, Y. Takazawa, K. Miyazaki, and T. Abe, *The Journal of Physical Chemistry C*, **114**, 11680 (2010).
- S.-K. Jeong, M. Inaba, Y. Iriyama, T. Abe, and Z. Ogumi, *Electrochemical and Solid-State Letters*, **6**, A13 (2003).
- Y. Yamada, K. Furukawa, K. Sodeyama, K. Kikuchi, M. Yaegashi, Y. Tateyama, and A. Yamada, *Journal of the American Chemical Society*, **136**, 5039 (2014).
- J. Wang, Y. Yamada, K. Sodeyama, C. H. Chiang, Y. Tateyama, and A. Yamada, *Nature Communications*, **7**, 12032 (2016).
- L. Suo, O. Borodin, T. Gao, M. Olguin, J. Ho, X. Fan, C. Luo, C. Wang, and K. Xu, *Science*, **350**, 938 (2015).
- J. M. Barthel, H. Krienke, and W. Kunz, *Physical chemistry of electrolyte solutions: modern aspects*, Springer Science & Business Media, 1998.
- C. Angell and R. Bressel, *The Journal of Physical Chemistry*, **76**, 3244 (1972).
- S. Smedley, *The interpretation of ionic conductivity in liquids*, Springer Science & Business Media, 2012.
- K. Izutsu, *Electrochemistry in nonaqueous solutions*, John Wiley & Sons, 2009.
- L. M. Varela, M. Garcia, F. Sarmiento, D. Attwood, and V. Mosquera, *Journal of Chemical Physics*, **107**, 6415 (1997).
- L. M. Varela, J. Carrete, M. Garcia, L. J. Gallego, M. Turmine, E. Rilo, and O. Cabeza, *Fluid Phase Equilibria*, **298**, 280 (2010).
- L. Varela, J. Carrete, J. Rodriguez, L. Gallego, M. Garcia, M. Turmine, and O. Cabeza, *Pseudolattice theory of ionic liquids*, INTECH Open Access Publisher, 2011.
- L. M. Varela, J. Carrete, M. Turmine, E. Rilo, and O. Cabeza, *Journal of Physical Chemistry B*, **113**, 12500 (2009).
- G. W. Murphy, *Journal of the Chemical Society, Faraday Transactions 2: Molecular and Chemical Physics*, **79**, 1607 (1983).
- A. Chagnes, B. Carré, P. Willmann, and D. Lemordant, *Electrochimica Acta*, **46**, 1783 (2001).
- B. Claude-Montigny, E. Rioteau, D. Lemordant, P. Topart, and G. Bossier, *Electrochimica Acta*, **47**, 533 (2001).
- A. Chagnes, B. Carré, P. Willmann, and D. Lemordant, *Journal of Power Sources*, **109**, 203 (2002).
- C. E. Woodward and K. R. Harris, *Physical Chemistry Chemical Physics*, **12**, 1172 (2010).
- H. Mercedes Villullas and E. R. Gonzalez, *Journal of Physical Chemistry B*, **109**, 9166 (2005).
- J. F. Casteel and E. S. Amis, *Journal of Chemical and Engineering Data*, **17**, 55 (1972).
- V. V. Shcherbakov, *Russian Journal of Electrochemistry*, **45**, 1292 (2009).
- G. Herlem, B. Fahys, M. Herlem, and J.-F. Penneau, *Journal of solution chemistry*, **28**, 223 (1999).
- C.-H. Yim, J. Tam, H. Soboleski, and Y. Abu-Lebdeh, *Journal of The Electrochemical Society*, **164**, A1002 (2017).
- C. Monnin, M. Dubois, N. Papaiconomou, and J.-P. Simonin, *Journal of Chemical & Engineering Data*, **47**, 1331 (2002).
- M.-Y. Li, L.-S. Wang, and J. Gmehling, *Industrial & Engineering Chemistry Research*, **50**, 3621 (2011).
- D. Li, D. Zeng, H. Han, L. Guo, X. Yin, and Y. Yao, *Calphad*, **51**, 1 (2015).
- M. Kobayashi and H. Tanaka, *Physical Review Letters*, **106**, 125703 (2011).
- D. Inman and D. G. Lovering, *Ionic liquids*, Springer Science & Business Media, 2013.
- W. Beichel, Y. Yu, G. Dlubek, R. Krause-Rehberg, J. Pionteck, D. Pfeifferkorn, S. Bulut, D. Bejan, C. Friedrich, and I. Krossing, *Physical Chemistry Chemical Physics*, **15**, 8821 (2013).
- K. Tanaka and R. Tamamushi, *Zeitschrift für Naturforschung A*, 141 (1991).
- S. Prasad, C. Chakravarty, and H. K. Kashyap, *Journal of Molecular Liquids*, **225**, 240 (2017).
- A. Hirata, L. J. Kang, T. Fujita, B. Klumov, K. Matsue, M. Kotani, A. R. Yavari, and M. W. Chen, *Science*, **341**, 376 (2013).
- N. P. Aravindakshan, C. M. Kuntz, K. E. Gemmell, K. E. Johnson, and A. L. L. East, *The Journal of Chemical Physics*, **145**, 094504 (2016).
- A. Y. Efimov, M. K. Khripun, L. A. Myund, and O. N. Pestova, *International Journal of Nanotechnology*, **13**, 95 (2016).
- H. Tanaka, *Faraday Discussions*, **167**, 9 (2013).
- M. De Graef and M. E. McHenry, *Structure of Materials: An Introduction to Crystallography, Diffraction and Symmetry*, Cambridge University Press, 2007.
- A. Chagnes, S. Nicolis, B. Carré, P. Willmann, and D. Lemordant, *ChemPhysChem*, **4**, 559 (2003).
- M. K. Khripun, Y. P. Kostikov, A. A. Kiselev, and O. N. Pestova, *Russian Journal of General Chemistry*, **74**, 167 (2004).
- M. B. Singh, V. H. Dalvi, and V. G. Gaikar, *RSC Advances*, **5**, 15328 (2015).
- A. Aouizerat-Elarby, H. Dez, B. Prevel, J. F. Jal, J. Bert, and J. Dupuy-Philon, *Journal of Molecular Liquids*, **84**, 289 (2000).
- J. L. Green, A. R. Lacey, and M. G. Sceats, *Chemical Physics Letters*, **134**, 385 (1987).
- R. L. McGreevy and M. A. Howe, *Journal of Physics: Condensed Matter*, **1**, 9957 (1989).
- K. J. Laidler and J. H. Meiser, *Physical Chemistry*, Benjamin/Cummings Publishing Company, 1982.
- P. R. Smirnov and V. N. Trostin, *Russian Journal of General Chemistry*, **76**, 175 (2006).
- L. E. Bove, C. Dreyfus, R. Torre, and R. M. Pick, *The Journal of Chemical Physics*, **139**, 044501 (2013).
- V. G. Artemov, A. A. Volkov, N. N. Syssoev, and A. A. Volkov, *EPL (Europhysics Letters)*, **109**(2), 26002 (2015).
- A. Annamareddy and J. Eapen, *Entropy*, **19**, 227 (2017).
- A. Annamareddy and J. Eapen, *Scientific Reports*, **7**, 44149 (2017).
- P. G. Bruce, *Solid state electrochemistry*, Cambridge University Press, 1997.
- Y. Yu, D. Bejan, and R. Krause-Rehberg, *Fluid Phase Equilibria*, **363**, 48 (2014).
- J. M. G. Cowie, A. C. S. Martin, and A.-M. Firth, *British Polymer Journal*, **20**, 247 (1988).
- M. Petrowsky and R. Frech, *Electrochimica Acta*, **55**, 1285 (2010).